Eur. Phys. J. C (2024) 84:1053
https://doi.org/10.1140/epjc/s10052-024-13211-9

THE EUROPEAN PHYSICAL JOURNAL C

Regular Article - Theoretical Physics

Herwig 7.3 release note

Gavin Bewick[1], Silvia Ferrario Ravasio[2], Stefan Gieseke[3], Stefan Kiebacher[3], Mohammad R. Masouminia[1], Andreas Papaefstathiou[4], Simon Plätzer[5,6], Peter Richardson[1], Daniel Samitz[7], Michael H. Seymour[8,a], Andrzej Siódmok[9], James Whitehead[10]

[1] IPPP, Department of Physics, Durham University, Durham, UK
[2] CERN, Theoretical Physics Department, Geneva, Switzerland
[3] Institute for Theoretical Physics, Karlsruhe Institute of Technology, Karlsruhe, Germany
[4] Department of Physics, Kennesaw State University, 830 Polytechnic Lane, Marietta, GA 30060, USA
[5] Theoretical Physics, NAWI Graz, University of Graz, Graz, Austria
[6] Particle Physics, Faculty of Physics, University of Vienna, Vienna, Austria
[7] Stefan Meyer Institute for Subatomic Physics, Austrian Academy of Sciences, 1010 Vienna, Austria
[8] Particle Physics Group, Department of Physics and Astronomy, University of Manchester, Manchester, UK
[9] Jagiellonian University, ul. prof. Stanisława Łojasiewicza 11, Kraków, Poland
[10] The Henryk Niewodniczański Institute of Nuclear Physics in Kraków, Polish Academy of Sciences, Kraków, Poland

Received: 12 July 2024 / Accepted: 6 August 2024

Abstract A new release of the Monte Carlo event generator Herwig (version 7.3) has been launched. This iteration encompasses several enhancements over its predecessor, version 7.2. Noteworthy upgrades include: the implementation of a process-independent electroweak angular-ordered parton shower integrated with QCD and QED radiation; a new recoil scheme for initial-state radiation improving the behaviour of the angular-ordered parton shower; the incorporation of the heavy quark effective theory to refine the hadronization and decay of excited heavy mesons and heavy baryons; a dynamic strategy to regulate the kinematic threshold of cluster splittings within the cluster hadronization model; several improvements to the structure of the cluster hadronization model allowing for refined models; the possibility to extract event-by-event hadronization corrections in a well-defined way; the possibility of using the string model, with a dedicated tune. Additionally, a new tuning of the parton shower and hadronization parameters has been executed. This article discusses the novel features introduced in version 7.3.0.

1 Introduction

Herwig, a multi-purpose event generator for reactions at pp, ep and ee colliders, is now available in a new version, 7.3. The Herwig 7 release series, started with [1] and continuing with [2,3], is based on the Herwig++ development [4–9] and fully supersedes the previous Herwig++ and HERWIG versions. The main cornerstones of the Herwig 7 series are significant improvements to the prediction of the hard scattering, now routinely available at next-to-leading order QCD, as well as major development and theoretical insight into the available angular-ordered and dipole parton shower algorithms and their accuracy. A major follow-up release of these previous Herwig 7 versions is now available as Herwig 7.3. The updates in this release are centred around parton shower algorithms, the hadronization model and soft QCD interactions in hadronic collisions. Please refer to the Herwig++ manual [4], the Herwig 7.0 [1] as well as this release note when using the new version of the program. Studies or analyses that rely on a particular feature of the program should also reference the paper(s) where the physics of that feature was first described. The authors are happy to provide guidance on which features are relevant for a particular analysis. A major publication intended as physics reference and manual will be appearing in the coming year.

1.1 Availability

The new version, as well as older versions of the Herwig event generator can be downloaded from the website https://herwig.hepforge.org/. We strongly recommend using the `bootstrap` script provided for the convenient installation of Herwig and all of its dependencies, which can be obtained from the same location. On the website, tutorials

[a] e-mail: michael.seymour@manchester.ac.uk (corresponding author)

Published online: 14 October 2024

and FAQ sections are provided to help with the usage of the program. Further enquiries should be directed to herwig@projects.hepforge.org. Herwig is released under the GNU General Public License (GPL) version 3 and the MCnet guidelines for the distribution and usage of event generator software in an academic setting, see the source code archive or http://www.montecarlonet.org/.

1.2 Prerequisites and further details

Herwig 7.3 is built on the same backbone and dependencies as its predecessors Herwig 7.0, 7.1 and 7.2, and uses the same method of build, installation and run environment. No major changes should hence be required in comparison to a working Herwig 7.2 installation. Some of the changes, though, might require different compiler versions. The tutorials at https://herwig.hepforge.org/tutorials/ have been extended and adapted to the new version and serve as the primary reference for physics setups and as a user manual until a comprehensive replacement for the detailed manual [4] is available.

In Herwig 7.3, one backward incompatibility has been introduced that will affect users' input files. The previous instance of QCD coupling, `AlphaQCD`, has been replaced by two instances. `AlphaQCDFSR` is used for processes with only final-state radiation, i.e. final-state parton showers, matrix element corrections to e^+e^- processes and partonic decays of final-state objects. `AlphaQCDISR` is used for all other processes, including initial-state parton showers and built-in matrix elements for hadron collisions. Users should change instances of `AlphaQCD` in their input files to `AlphaQCDISR`, unless they are specifically targeted at e^+e^- or other final-state effects such as top quark decays, in which case they should use `AlphaQCDFSR`.

2 Improvements on the angular ordered parton shower

Process-independent parton showers have long been one of the pivotal components in all multi-purpose event generators for particle physics. One of the key features of Herwig 7 has been the provision of two complementary paradigms for parton showering: the angular ordered parton shower and the transverse momentum ordered dipole shower. Version 7.3 includes significant improvements to the angular ordered parton shower, including electroweak radiation for the first time, and improving the method by which partons' kinematics are reconstructed at the end of the shower (the recoil scheme).

Predominantly, the current paradigm for parton showers revolves around the QCD+QED schemes, which, while yielding satisfactory results in present conditions, might not be sufficient as we approach higher energy scales where it is anticipated that EW bosons will begin to manifest as massless partons, a prediction corroborated by recent LHC observations [10,11]. Further compelling evidence for this shift is found in the corresponding electroweak virtual corrections, which are both substantial and predominantly negative. These observations and findings underline the pressing need to innovate beyond the current status quo. There exists a strong justification for the introduction of a process-independent EW parton shower, essentially pushing the envelope and evolving the parton shower framework to a more comprehensive QCD+QED+EW scheme [12].

The Herwig angular-ordered parton shower dresses the hard event with a series of iterated $1 \to 2$ ordered branchings. When a new emission is generated, it is necessary to perform momentum reshuffling to assign virtuality to the pre-branching emitter, allowing the splitting. This procedure makes it impossible to preserve all the kinematic invariants associated with previous branchings. The choice of the preserved variable defines the recoil scheme. Since the ordering scale can be expressed in terms of the preserved variable, the recoil scheme coincides with the interpretation of the ordering variable. Herwig 7.2 featured three recoil schemes for final-state radiation (FSR): the transverse-momentum preserving scheme [13], the virtuality-preserving scheme [14], and the so-called "dot-product" preserving scheme [15]. This latter scheme preserves the dot product between the momenta of the post-branching partons originating from the splitting. Initial-state radiation (ISR) was always reconstructed using the transverse-momentum recoil scheme [13]. Version 7.3 enables the consistent use of all three schemes for FSR and ISR [16]. The dot-product preserving scheme is now the default for both ISR and FSR.

2.1 Process-independent electroweak radiation

Using the fundamental shower kinematics and dynamics of Herwig 7 in the *quasi*-collinear limit [4,12,17] while assuming a generic splitting $\widetilde{ij} \to i + j$ for the quark splittings:

$$q \to q' W^{\pm}, \quad q \to q Z^0, \tag{1}$$

$$q \to q H, \tag{2}$$

as well as the EW gauge boson splittings:

$$W^{\pm} \to W^{\pm} Z^0, \quad W^{\pm} \to W^{\pm} \gamma, \quad Z^0 \to W^+ W^-, \quad \gamma \to W^+ W^-, \tag{3}$$

$$W^{\pm} \to W^{\pm} H, \quad Z^0 \to Z^0 H, \tag{4}$$

one can write the helicity amplitudes of $\widetilde{ij} \to i + j$ in the *quasi*-collinear limit as:

$$H_{\widetilde{ij} \to i+j}(z, \tilde{q}; \lambda_{\widetilde{ij}}, \lambda_i, \lambda_j) = g \sqrt{\frac{2}{\tilde{q}^2_{\widetilde{ij}} - m^2_{\widetilde{ij}}}} F^{\widetilde{ij} \to i+j}_{\lambda_{\widetilde{ij}}, \lambda_i, \lambda_j}, \tag{5}$$

where $\tilde{q}$ denotes the evolution scale of the shower, and $m_{\tilde{ij}}$ the mass of progenitor. Additionally, the vertex function $F^{\tilde{ij}\to i+j}_{\lambda_{\tilde{ij}},\lambda_i,\lambda_j}$ is derived exclusively from Feynman rules [12]. Consequently, the splitting function can be delineated as:

$$P_{\tilde{ij}\to i+j}(z,\tilde{q}) = \sum_{\text{spins}} \left| H_{\tilde{ij}\to i+j}(z,\tilde{q};\lambda_{\tilde{ij}},\lambda_i,\lambda_j) \right|^2, \tag{6}$$

and explicit expressions for Eq. (6) can be given for the splittings (1)–(4) as:

$$\begin{aligned} P_{q\to q'V}(z,\tilde{q}) = \frac{1}{1-z}\Bigg[& \left({g_L}^2\rho_{-1,-1} + {g_R}^2\rho_{1,1}\right) \\ & \times \left\{ (1+z^2)\left(1+\frac{m_0^2}{\tilde{q}^2 z(1-z)}\right) - \frac{m_1^2(1+z)}{z\tilde{q}^2(1-z)} \right. \\ & \left. - \frac{m_2^2}{z\tilde{q}^2} \right\} + \frac{{m_0}^2}{\tilde{q}^2}\left({g_L}^2\rho_{1,1} + {g_R}^2\rho_{-1,-1}\right) \\ & - \frac{2m_0 m_1}{z\tilde{q}^2} g_L g_R \left(\rho_{1,1}+\rho_{-1,-1}\right) \Bigg], \end{aligned} \tag{7}$$

$$P_{q\to qH}(z,\tilde{q}) = g^2\left(\frac{m_0}{m_W}\right)^2\left[(1-z)+\frac{4m_0^2-m_2^2}{\tilde{q}^2(1-z)z}\right], \tag{8}$$

$$\begin{aligned} P_{V\to V'V''}(z,\tilde{q}) = \frac{2(\rho_{-1,-1}+\rho_{1,1})}{(1-z)z}\Big[& (1-(1-z)z)^2 \\ & + m_{0,t}^2(1-(1-z)z)^2 - m_{1,t}^2(1-(1-z)z^2) \\ & - m_{2,t}^2(1-(1-z)^2 z) + 2\rho_{0,0}m_{0,t}^2 z(1-z)^3\Big], \end{aligned} \tag{9}$$

$$\begin{aligned} P_{V\to VH}(z,\tilde{q}) = & \frac{1-z}{4z}\left[z^2(\rho_{-1,-1}+\rho_{1,1})+2\rho_{0,0}\right] \\ & - \frac{m_{H,t}^2}{4z}\left[z^2(\rho_{-1,-1}+\rho_{1,1})+2\rho_{0,0}\right] \\ & - \frac{m_{0,t}^2}{4z^2}\Big[\left(2z^2-4z+2\right)\rho_{0,0} \\ & + \left(z^4-2z^3-z^2\right)(\rho_{-1,-1}+\rho_{1,1})\Big], \end{aligned} \tag{10}$$

with m_k, $k = 0,\ 1,\ 2$ being the masses of the particles $\tilde{ij}$, i, j respectively and $m_{k,t}^2 = m_k^2/(\tilde{q}^2 z(1-z))$. Note that the expressions above are derived using Dawson's approach [18]. In this approach, terms in the longitudinal polarization vectors of the EW vector bosons, which are proportional to their momenta, are systematically removed to prevent irreducible divergences in the resulting splitting functions [12].

On the development side, the helicity-dependent splitting kernels for (1)–(4) are introduced into Herwig 7's AO parton shower though the introduction of four new classes, namely `HalfHalfOneEWSplitFn`, `HalfHalfZeroEWSplitFn`, `OneOneOneEWSplitFn` and `OneOneZeroEWSplitFn` respectively. The first two can by default contribute to both initial and final state radiation, while the latter two are explicitly final state splittings. This is because the inclusion of backward EW vector boson evolution in the initial state parton shower requires the use of EW parton distribution functions, which will reduce the generality and efficiency of the algorithm and does not increase its reliability.

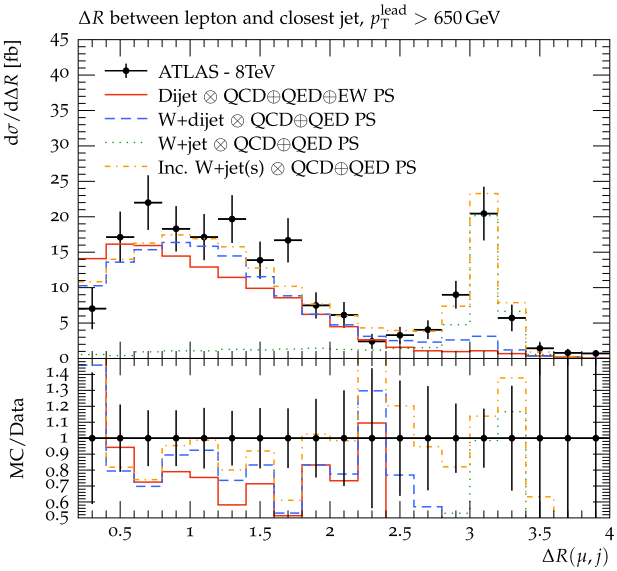

Fig. 1 Angular distribution of a W boson in association with a leading jet possessing transverse momentum greater than 650 GeV, observed at a center-of-mass energy of 8 TeV, as detailed in [12]

Additionally, each weakly interacting progenitor in the AO shower is now tagged with an EW scale, alongside QCD and QED scales, allowing for a seamless interleaving of these interactions via the new `QCD+QED+EW` default scheme. This choice can be altered via the following interface commands

```
cd /Herwig/Shower
set ShowerHandler:Interactions <scheme>
```

Here, the option `ALL` corresponds to the `QCD+QED+EW` shower scheme. The other available options are `QEDQCD`, `QCD`, `QED` and `EWOnly`.

The performance and physics of this new iteration of the AO parton shower has been comprehensively validated in [12] and its phenomenology in producing credible predictions against experimental observations has been surveyed in [19,20].

As an example, Fig. 1 [12] shows the angular distribution of $W^{\pm}$ bosons and high-p_t jets at a center-of-mass energy of 8 TeV, using ATLAS data [21]. It specifically highlights the distribution of muons relative to the nearest jet with a transverse momentum greater than 650 GeV. The blue dashed and green dotted lines represent simulations with $W^{\pm} + jet$ and $W^{\pm} + 2jets$ matrix elements (MEs), respectively, and the orange dash-dotted line is the combined result of these two MEs. These MEs were created with MadGraph [22] and then processed with `Herwig`'s `QCD+QED` showering scheme. The red solid line, however, is derived from a pure QCD dijet event showered using `Herwig`'s comprehensive

QCD+QED+EW scheme. The proximity of the red histogram to the blue in this Figure showcases the effectiveness of Herwig's QCD+QED+EW parton shower scheme in accurately reproducing the angular distribution of $W^{\pm}$ bosons with high-p_t jets, even without explicit W emissions from the hard process.

2.2 Dot-product preserving recoil scheme

The Herwig angular-ordered parton shower algorithm [13] is built on the Lorentz-invariant variables z and $\tilde{q}^2$, where z specifies the momentum sharing between the children in a $q_0 \to q_1 + q_2$ branching:

$$z = \frac{q_1 \cdot n}{q_0 \cdot n}, \tag{11}$$

where n is an auxiliary light-like vector specifying the collinear direction, and $\tilde{q}$ generalizes the emitter energy times opening angle,[1]

$$\tilde{q}^2 = \frac{q_0^2}{z(1-z)}. \tag{12}$$

The algorithm works by generating a $(z, \tilde{q}^2)$ pair for a branching, then allowing each of its children to probabilistically evolve and generate further branching, until a termination condition is reached. For a branching in which the children do not branch further, so are on their mass shell, Eqs. (11, 12) are unambiguous. The transverse momentum of the branching can be calculated,

$$p_T^2 = z^2(1-z)^2\tilde{q}^2, \tag{13}$$

and the kinematics reconstructed.

However, Eq. (12) is not the unique definition of $\tilde{q}^2$. When the children are on-shell, it can be written in any of the equivalent forms

$$\tilde{q}^2 = \frac{p_T^2}{z^2(1-z)^2} = \frac{q_0^2}{z(1-z)} = \frac{2q_1 \cdot q_2}{z(1-z)}. \tag{14}$$

When the children have acquired a non-vanishing virtuality through their subsequent evolution, we can continue to use Eq. (11), but we can choose to use only one of the three definitions of $\tilde{q}^2$ in Eq. (14) and the value of p_T^2 that is reconstructed for a given $\tilde{q}^2$ value will be different in each case.

The original choice of Ref. [13] was to use Eq. (13), which we now call the **p_T-preserving scheme**.

[1] To simplify the presentation here, we neglect parton masses, but they are fully implemented in the algorithm [15] and code. We also describe the algorithm only for final-state evolution, but again it is fully implemented also for initial-state evolution [16].

In Ref. [14], it was pointed out that the p_T-preserving scheme gives too much hard radiation, as the virtuality of the parent parton can grow arbitrarily after multiple emissions. It was suggested that an alternative scheme, based on the second of the options in Eq. (14) does not suffer this problem. We call this the **q^2-preserving scheme**. It results in

$$p_T^2 = z^2(1-z)^2\tilde{q}^2 - q_1^2(1-z) - q_2^2 z, \tag{15}$$

which is clearly smaller when there is subsequent emission, resulting in a less strong growth of virtuality after multiple emissions and a better description of LEP data at $\sqrt{s} = M_{Z^0} = 91.1876$ GeV. However, it was found that this definition sometimes results in events that should have a negative p_T^2 according to this formula, so cannot be reconstructed. This was remedied by replacing p_T by zero in those events. However, in Ref. [15], it was shown that the adoption of the q^2-preserving scheme results in a formal loss of logarithmic accuracy. A third scheme, the **dot-product $(q_1 \cdot q_2)$ preserving scheme** was then defined, based on the third option in Eq. (14). It results in

$$p_T^2 = z^2(1-z)^2\tilde{q}^2 - q_1^2(1-z)^2 - q_2^2 z^2. \tag{16}$$

We can see that this is intermediate between the other two schemes and is found to have a 'best of both' behaviour: the virtuality does not grow excessively in multiple emissions, but remains within the kinematically reconstructible phase space and maintains the same formal logarithmic accuracy of the p_T-preserving formulation, which reaches Next-to-Leading Logarithms for global observables, such as event shapes.

The dot-product preserving scheme was extended to initial-state evolution in Ref. [16]. When an incoming parton q_1 backward-evolves into a parton q_0 (emitting a final-state parton q_2), the ordering variable can be written as

$$\tilde{q}^2 = \frac{p_T^2}{(1-z)^2} = \frac{-q_1^2}{1-z} = \frac{2q_0 \cdot q_2}{1-z}. \tag{17}$$

It was noted that in the case of ISR, subsequent emissions tend to increase the value of p_T^2 because incoming partons develop a negative virtuality, in contrast to the FSR case, where new emissions tend to decrease p_T^2. Tuning the strong coupling constant α_s using the transverse-momentum distribution of the Z boson measured at the LHC, which is primarily sensitive to ISR, results in a value larger than the one obtained from LEP data, that instead exclusively probes FSR. For this reason we introduced separate values of α_s for ISR and FSR. The previous instance of AlphaQCD has now been replaced by two instances, AlphaQCDFSR and AlphaQCDISR. AlphaQCDISR is used for the initial-state shower and for built-in matrix elements for hadron collisions,

while AlphaQCDFSR is used for the final-state shower, matrix element corrections to built-in matrix elements for e^+e^- and for final-state decays. Their input values (defined in the CMW scheme[23] at M_{Z^0}) can be set by

```
cd /Herwig/Shower
set AlphaQCDISR:AlphaIn <value>
set AlphaQCDFSR:AlphaIn <value>.
```

All three schemes are now available in Herwig 7.3 for both ISR and FSR, with the dot-product preserving scheme the default. The recoil scheme can be selected with the interface commands

```
cd /Herwig/Shower
set ShowerHandler:EvolutionScheme
  <scheme>
```

and if necessary

```
set PowhegShowerHandler:EvolutionScheme
  <scheme>
```

where <scheme> is pT, Q2 or DotProduct. We encourage the use of the transverse-momentum preserving scheme to estimate shower uncertainties induced by the recoil scheme, but we discourage the use of the virtuality-preserving scheme, as it deteriorates the formal logarithmic accuracy of the angular-ordered shower. For this reason, the phenomenological study carried out in Ref. [16] does not include this latter scheme. In Fig. 2 we compare the transverse-momentum distribution of the Z boson produced in proton–proton collisions at $\sqrt{s} = 8$ TeV with the predictions obtained using the Herwig angular-ordered shower for the dot-product (red) and p_T (blue) recoil schemes. We notice that the two schemes, which both reach next-to-leading logarithmic accuracy for this observable, are in good agreement between each other and with ATLAS data [24].

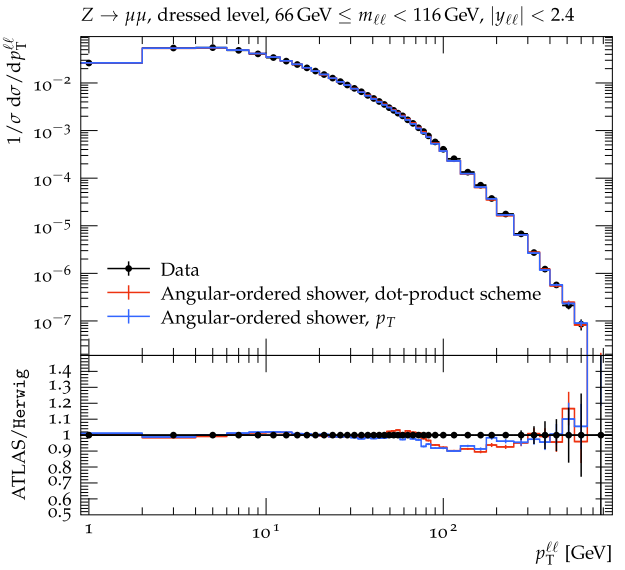

Fig. 2 Transverse momentum distribution of a Z boson decaying into a pair of dressed muons in proton–proton collisions at $\sqrt{s} = 8$ TeV. The data is from the ATLAS Collaboration [24]. The red curve is given by the Herwig angular-ordered shower with the dot-preserving scheme (default as from version 7.3), while the blue curve uses the transverse-momentum (p_T) scheme. Both curves are obtained using Matrix-Element-Corrections to describe the hardest emission, and the shower parameters are those from Ref. [16]

3 Developments of the cluster hadronization and secondary decay models

3.1 HQET in hadronization and decay of heavy and excited hadrons

The enhancement of the transmission of heavy hadron polarization post-parton shower is pivotal for predicting heavy hadron behaviour in high-energy collisions. When the heavy quark mass m_Q is significantly greater than the QCD scale Λ_{QCD}, light degrees of freedom become insensitive to the mass, leading to crucial implications for the isospin heavy hadron multiplets $(H, H^\star)$. In the context of HQET, it is found that the existence of a strong hierarchy between the ground state decay width $\Gamma(H \to X)$, multiplet mass splitting Δm and the decay width of the radiative decay $\gamma(H^\star \to HX)$:

$$\Gamma(H \to X) \gg \Delta m \gg \gamma(H^\star \to HX), \tag{18}$$

could result in heavy quarks acting as static colour sources. This facilitates the emergence of a "spin-flavour symmetry" for heavy quarks. Meanwhile, the Falk-Peskin "no-win" theorem [25] elucidates the limits of polarization information retrieval:

$$\Delta m \gg \Gamma \gg \gamma \quad \text{or} \quad \Delta m \gg \gamma \gg \Gamma,$$

implying that polarization details are lost in non-excited mesons under these conditions. This finding extends to other cases within similar hierarchies of mass splitting and decay widths.

The above-mentioned spin-flavour symmetry facilitates model-independent predictions for heavy hadron spectra and interactions, separating short-distance perturbative interactions from long-distance non-perturbative fragmentation processes. As a consequence, the attributes of the heavy quark – such as velocity, mass, and spin – remain largely unaffected by the dynamics of light quarks in the hadronization sequence. This separation of scales allows the preservation of heavy quark polarization, which could be reflected in the spin polarization of produced heavy mesons and baryons. However, this can be influenced by the light quark's angular momentum and parity-conserving fragmentation processes that may lead to anisotropies, characterized by a model-dependent parameter ω_j.

For the D_1 and $D_2^\star$ meson states, considering the left-handed polarization of the charm quark, the light degrees of freedom with $j_q = \frac{3}{2}$ can exhibit any of the four helicity states. Due to parity invariance, the probability of forming a specific helicity state is independent of the helicity's sign but can vary for different helicity magnitudes. The parameter ω_j is introduced to denote the likelihood of fragmentation into a state with the maximum $|j_q^{(3)}|$ value. This allows for a breakdown of the probabilities for various helicity states, demonstrating how the combination of a left-handed charm quark with particular light quark helicities leads to distinctively populated helicity states with their respective probabilities for D, $D_0^\star$, D_1, and $D_2^\star$.

To determine the numerical value of ω_j, we consider the amplitude for the production of a pion at θ, ϕ from a $H^\star \to H\pi$ type meson decay, which is proportional to the spherical harmonics $Y_j^\ell(\theta, \phi)$

$$\frac{d\Gamma(H^\star \to H\pi)}{d\cos\theta} \propto \int d\phi \sum_j P_{H^\star}(j)\left|Y_j^\ell(\theta,\phi)\right|^2, \tag{19}$$

Here, ℓ is the angular momentum quantum number of $H^\star$ and $P_{H^\star}(j)$ is the probability of a $H^\star$ emerging with helicity j [26]. For instance, the differential decay width for $D_2^\star \to D\pi$ has been analyzed against experimental data, establishing an upper limit of $\omega_{3/2} < 0.24$ at 90% CL [25]. In Herwig 7.3, we incorporate a `SpinHadronizer` class, particularly its sub-function `mesonSpin`, to systematically assign spin and polarization to newly formed mesons based on the heavy quark's flavour and the meson's spin attributes, with a default value of $\omega_{3/2} = 0.20$ [26].

An analogous examination applies to heavy baryons. For these, the ground state is defined by a heavy quark paired with a light diquark system, which has a helicity of $j_{qq} = 0$. In such a state, no angular momentum is imparted to the heavy quark, thus the original polarization remains unaffected. Therefore, the initial polarization of the heavy quarks can be expected to directly affect the ground state polarization of heavy baryons. The likelihood of encountering these states during the fragmentation of heavy sectors continues to be dictated by two specific parameters, ω_a and ω_j. Here, ω_a denotes the probability of forming a $j_{qq} = 1$ diquark in contrast to a $j_{qq} = 0$ ground state setup. Within the framework of Herwig 7's cluster hadronization approach, ω_a is set to 1, reflecting an unbiased probability between the formation of spin-0 and spin-1 diquarks [26]. The numerical value of ω_1 can be estimated similar to the case of $\omega_{3/2}$, considering the decay widths of the observed decay modes $\Sigma_c \to \Lambda_c\pi$ and $\Sigma_c^\star \to \Lambda_c\pi$, which results in $\omega_1 = 2/3$.

The above arguments allow one to determine the polarization distributions of the excited heavy mesons and heavy baryons, through the helicity state of their heavy quark constituents, as described in [26]. The explicit results for the case of excited heavy mesons and heavy baryons are tabulated in Tables 1 and 2.

At this stage, it is crucial to note that due to the scarce experimental data around these heavy hadrons, we depend heavily on the principles of HQET to predict how they decay, including their lifetimes and decay modes, as it lays down fundamental connections between the coupling constants involved in these decays. HQET has been already used for modeling the strong and radiative decay of heavy baryons, as shown in some prior studies and its integration into Herwig++ [4]. Nevertheless, we still have to develop such a prescription for the heavy meson sector. We begin by identifying the $s-$ and $p-$wave meson multiplets: the ground state doublets ($J^P = 0^-, 1^-$) including D and $D^\star$ mesons, the $J^P = 1^+, 2^+$ doublet with D_1 and $D_2^\star$ mesons, and the $J^P = 0^+, 1^+$ doublet comprising $D_0^\star$ and D_1' mesons [27]. We also account for the mixing effects between D_1 and D_1' mesons resulting from higher-order corrections in HQET. The methodology and notation for calculating the matrix elements associated with meson decays are as per Falk et al. [27,28], with a focus on balancing theoretical precision with empirical data representation. The matrix elements are defined by equations (20) through (25) below, incorporating decay parameters and polarization vectors, where p_i denotes the hadron momenta and ϵ_i the polarization vectors [26]. Here, the index $i = 0$ identifies the parent hadron, while $i = 1$ and $i = 2$ refer to the resulting heavy and light daughter hadrons. The mass of a hadron H is represented by m_H. The parameters g, h, Λ, f_π and f'' are constants associated with the decay process. Furthermore, θ_q is introduced as the mixing angle between the meson pairs (D_1, D_1') and (D_{s1}, D_{s1}').

$$\mathcal{M}(D^\star \to D\pi) = -\frac{2g}{f_\pi}\left(m_D m_{D^\star}\right)^{\frac{1}{2}} p_0 \cdot \epsilon_0, \tag{20}$$

$$\mathcal{M}(D_2^\star \to D\pi) = -\frac{2h}{f_\pi \Lambda}\left(m_{D_2} m_D^\star\right)^{\frac{1}{2}} \epsilon_0^{\mu\nu} p_{0,\mu} p_{0,\nu}, \tag{21}$$

$$\mathcal{M}(D_2^\star \to D^\star\pi) = -i\frac{2h}{f_\pi \Lambda}\left(\frac{m_{D^\star}}{m_{D_2}}\right)^{\frac{1}{2}} \epsilon^{\alpha\beta\mu\nu}\epsilon^0_{\alpha\gamma} p_0^\gamma p_{0,\mu} p_{1\nu}\epsilon_{1\beta}, \tag{22}$$

$$\mathcal{M}(D_1 \to D^\star\pi) = \frac{h}{f_\pi \Lambda}\left(\frac{2}{3} m_{D_1} m_D\right)^{\frac{1}{2}} \times\left[\epsilon_0\cdot\epsilon_1\left(p_0^2 - \left[\frac{p_0\cdot p_1}{m_0}\right]^2\right) - 3\epsilon_0\cdot p_0\epsilon_1\cdot p_0\right], \tag{23}$$

$$\mathcal{M}(D_0^\star \to D\pi) = \frac{f''}{f_\pi}\left(m_{D_0^\star} m_D\right)^{\frac{1}{2}} p_0\cdot\left(\frac{p_1}{m_{D_0^\star}} + \frac{p_2}{m_D}\right), \tag{24}$$

$$\mathcal{M}(D_1' \to D^\star\pi) = -\frac{f''}{f_\pi}\left(m_{D_1'} m_D\right)^{\frac{1}{2}}\left[-p_0\cdot\left(\frac{p_1}{m_{D_0^\star}} + \frac{p_2}{m_D}\right)\epsilon_0\cdot\epsilon_1 + \frac{1}{m_{D_1'}}\epsilon_1\cdot p_1\epsilon_0\cdot p_0 + \frac{1}{m_D}\epsilon_0\cdot p_2\epsilon_1\cdot p_0\right]. \tag{25}$$

Table 1 Polarization states of charmed mesons, D, $D^\star$, D_1 and $D_2^\star$ [26]

$\hat{\rho}$	$\rho_{0,0}$	$\rho_{1,1}$	$\rho_{2,2}$	$\rho_{3,3}$	$\rho_{4,4}$
D	1	–	–	–	–
$D^\star$	$\frac{1}{2}(1-\rho_Q)$	$\frac{1}{2}$	$\frac{1}{2}(1+\rho_Q)$	–	–
D_1	$\frac{1}{16}[1-\rho_Q+\omega_{\frac{3}{2}}(3-5\rho_Q)]$	$\frac{1}{4}(1-\omega_{\frac{3}{2}})$	$\frac{1}{16}[1-\rho_Q+\omega_{\frac{3}{2}}(3+5\rho_Q)]$	–	–
$D_2^\star$	$\frac{1}{4}\omega_{\frac{3}{2}}(1-\rho_Q)$	$(\frac{3}{16}-\frac{1}{8}\omega_{\frac{3}{2}})(1-\rho_Q)$	$\frac{1}{4}(1-\omega_{\frac{3}{2}})$	$(\frac{3}{16}-\frac{1}{8}\omega_{\frac{3}{2}})(1+\rho_Q)$	$\frac{1}{4}\omega_{\frac{3}{2}}(1+\rho_Q)$

Table 2 Possible polarization states of charmed baryons, Λ_c, Σ_c and $\Sigma_c^\star$ [26]

$\hat{\rho}$	$\rho_{0,0}$	$\rho_{1,1}$	$\rho_{2,2}$	$\rho_{3,3}$
Λ_c	$\frac{1}{2}(1-\rho_Q)$	$\frac{1}{2}(1+\rho_Q)$	–	–
Σ_c	$\frac{1}{2}(1-\rho_Q)+\omega_1\rho_Q$	$\frac{1}{2}(1+\rho_Q)-\omega_1\rho_Q$	–	–
$\Sigma_c^\star$	$\frac{3}{8}\omega_1(1-\rho_Q)$	$\frac{1}{2}(1-\rho_Q)-\frac{1}{8}\omega_1(3-5\rho_Q)$	$\frac{1}{2}(1-\rho_Q)-\frac{1}{8}\omega_1(3+5\rho_Q)$	$\frac{3}{8}\omega_1(1+\rho_Q)$

With the established matrix elements for the decays at hand, we are equipped to determine the partial decay widths of the relevant two-body decay processes. To align our theoretical framework with the practical applications within Herwig 7, it is imperative to consider certain non-dominant terms that become significant in the context of the heavy quark expansion. In practical terms, this is described by:

$$\Gamma(H^* \to H\pi) = \frac{1}{8\pi m_{H^*}^2} \left|\mathcal{M}(H^* \to H\pi)\right|^2 p_{\mathrm{CM}}, \quad (26)$$

where p_{CM} is the momentum of the decaying particle in the center-of-mass system of the decayed two-body system. The resulting partial widths are reported in [26].

We calculated the decay parameters using recent measurements of charmed meson masses and decay widths. These parameters are important for understanding how these particles transform into others over time. Table 3 lists the best-fit values for these parameters.

Note that some mesons have decay modes that do not conserve isospin strongly. These modes become important when the usual isospin-conserving decays are not allowed or are very unlikely. We pay particular attention to the $D^\star$ mesons, which have various decay possibilities because of their energy levels. Our methods for examining these decays can also be applied to other mesons [26].

To integrate the processes of strong and radiative decays for excited heavy mesons into Herwig 7, we have created two dedicated classes: `HQETStrongDecayer` and `HQETRadiativeDecayer`. The decay parameters, emphasized in this segment, are set as variables that users can modify. Such an arrangement offers adaptability, allowing for adjustments and enhancements in line with new findings or needs. The efficacy of using HQET and spin-flavour symmetry to predict polarization-sensitive measurements has been extensively discussed in [26], see e.g. Fig. 3.

Table 3 Fitted values of the decay parameters

Parameter	Fitted value
f''	-0.465 ± 0.017
f_π	0.130 ± 0.001 [GeV]
h	0.824 ± 0.007
Λ	1.000 ± 0.000 [GeV]
g	0.565 ± 0.006
$\theta_{u,d}$	0.000 ± 0.100
θ_s	-0.047 ± 0.002

3.2 Improved cluster splitting dynamics

In Herwig 7's cluster hadronization model, the dynamics of hadron formation are conceptualized as a multi-step process, beginning with fragmentation and culminating in the production of observable hadrons. Initially, during fragmentation, coloured partons, produced in the primary hard process and the subsequent parton shower, are paired to form colour-neutral clusters. This pairing typically involves a quark with an antiquark, often originating from the breaking of colour flux tubes via the insertion of quark-antiquark pairs. Once formed, these clusters represent temporary and unstable com-

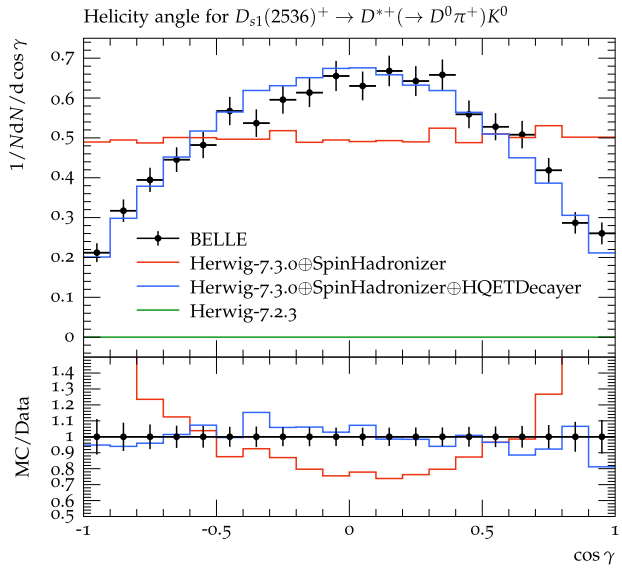

Fig. 3 Efficiency-corrected decay rates for $D_{s1} \to D^{\star+}K^0$ decay mode as a function of the angle (γ) between π^+ and K^0 in the $D^{\star+}$ rest frame. The data is from BELLE Collaboration [29]. The plot is from [26]

binations of partons. The subsequent step involves the decay or splitting of these clusters into final-state hadrons. For lighter clusters, this might involve a direct transformation into a meson or baryon. However, heavier clusters typically undergo a series of successive splittings until they reach configurations suitable for direct conversion into observable hadrons. This is handled by the `ClusterFissioner` class.

Each of these cluster splittings or decays is governed by the kinematic checks over the parent and children clusters, primarily focusing on the relation between the masses of the clusters and their constituent quarks. Formerly, Herwig 7.2 and older versions used only a static kinematic threshold for 2-body cluster splittings

$$M_0 > M_1 + M_2, \quad M_1 > m + m_1, \quad M_2 > m + m_2, \quad (27)$$

with M_i being the masses of the parent and children clusters. $m_{1,2}$ are the masses of the parent cluster's constituent quarks and m is the quark mass of a perturbatively spawned light quark-antiquark pair. Aiming to improve the kinematics of cluster splitting, Herwig 7.3 by default employs a new dynamic kinematic threshold scheme, in addition to keeping the static option available:

```
cd /Herwig/Hadronization
set ClusterFissioner:KinematicThreshold
  <Static/Dynamic>
```

The `Dynamic` choice updates the condition (27) with [26]

$$M_0^2 > M_1^2 + M_2^2, \quad M_1^2 > m^2 + m_1^2 + \delta_{\text{th}},$$

$$M_2^2 > m^2 + m_2^2 + \delta_{\text{th}}, \quad (28)$$

where the `KineticThresholdShift` parameter δ_{th} allows one to adjust this threshold through tuning. In this new regime, satisfaction of the condition (28) is not sufficient to allow for a cluster to split; an additional decision-making device in the form of a scale-dependent threshold-modulated probability distribution has been introduced:

$$P_{\text{cluster}} = \frac{1}{1 + |(M - \delta)/M_{\text{th}}|^r} > \text{Random}[0, 1], \quad (29)$$

where M_{th} signifies the cluster's mass threshold – the aggregate of the masses of the inherent quarks and the produced di-quark. The splitting is allowed only if P_{cluster} is greater than a random number between [0, 1]. The parameters δ and r may be chosen in a way to reduce the chance of splitting in successive instances.

Collectively, the addition of these three tunable parameters, namely `ProbabilityPowerFactor` (r), `ProbabilityShift` (δ), and `KineticThresholdShift` (δ_{th}) allows the user to exert further control over the cluster splittings [26]. This significant change required a new tune of Herwig 7.3 to the data, which will be addressed in Sect. 4.

3.3 New infrastructure for hadronization models

Several improvements are in development with respect to the cluster hadronization and will soon be available with an upcoming Herwig release, among them a dynamic cluster model [30] and other options for an improved understanding of hadronization. Many of the structures already appear in this release and allow for the flexible adjustment of kinematics and mass distributions in the cluster fission process (offering more alternatives to the choices made in Sect. 3.2), as well as the generation of dynamic gluon masses using the `GluonMassGenerator` class.

3.4 Event-by-event hadronization corrections

As part of the hadronization improvements, a new strategy has been developed to transfer the assignment of constituent masses entirely into the hadronization. Not only does this allow to have a consistent physics interface to the string model, but it also provides the possibility to extract event-by-event hadronization corrections in a clean way, i.e. a parton level which is not 'contaminated' by the non-perturbative constituent mass parameters. This is achieved by reshuffling the partonic ensemble to different mass shells at the beginning of the hadronization. While this can, in principle, be done across the entire event, the more physical choice is

to perform the reshuffling within colour singlet subsystems which will branch into clusters:

```
cd /Herwig/Hadronization
set ClusterHadHandler:Reshuffle Yes
set ClusterHadHandler:ReshuffleMode
  ColourConnected
cd /Herwig/Shower
set ShowerHandler:UseConstituentMasses
  No
```

The intermediate partonic state is then tagged by a status code which can be chosen at the level of the input file, and is available for analysis by reading it out from the event record:

```
cd /Herwig/Shower
set ShowerHandler:TagIntermediates
  <status code>
```

3.5 Particle data update

In Herwig 7.3.0, we have undertaken the first substantial update of particle data since the initial launch of Herwig 7. This update incorporates the latest findings from the Particle Data Group (PDG) 2022 review [31], marking a significant enhancement from the previously used PDG 2006 data [32]. Updated elements include particle masses, decay widths, decay modes, and branching ratios, ensuring that the users have access to simulations that employ the most up-to-date and accurate particle physics data available.

3.6 String hadronization tune with colour reconnection

With the new version of Herwig, we add the possibility of using the Lund string model for hadronization in both e^+e^- and pp collisions. The interface of the string model of Pythia 8 is provided via the P8I C++ package (written by L. Lönnblad) [33]. While the default version of the P8I is sufficient for hadronization of electron–positron collisions, we had to extend it to account for Colour Reconnection which is needed for realistic simulation of hadron-hadron collisions. The Lund string model, together with the angular ordered parton shower model, has been tuned to LEP and LHC data sets. Therefore, it is now possible to use the angular ordered parton shower of Herwig together with two different hadronization models, which may help estimate the differences associated with hadronization effects. Details will be described in a forthcoming publication.

4 Herwig 7.3 general tune

As with previous versions, we have tuned Herwig 7.3 using e^+e^- data from the LEP, PETRA, SLAC, SLC and TRISTAN measurements for over 9,200 individual data bins, weighted around both light and heavy hadron production rates and multiplicities, alongside a number of dominant processes. We have explored 12 parameters in total, with 10 related to cluster hadronization and the remaining 2, specifically `AlphaIn` and `pTmin`, associated with the AO parton shower. Due to the large number of relevant parameters and the sensitivity of their collective phase space, we opted for a multi-layered, brute-force tuning approach employing the `prof2-chisq` module of ProfessorII [34], aiming to minimize χ^2 value as a benchmark for optimal tuning [26].

The first layer (1000 samples) was probed around the whole viable phase space, with the lower threshold chosen to be the χ^2 of the tuned Herwig 7.2.3. The benchmark closest to the threshold was then chosen for the second layer, with the relative sampling phase space being tightened around it by 50%. After five layers of successive sampling, our strategy delivered a marked enhancement in the overall χ^2 value. Specifically, the tuned Herwig 7.3 achieved a roughly 50% χ^2 improvement over Herwig 7.2 and approximately 13% improvement against Herwig 7.2.3. The parameter content and the result of this new general tune for Herwig 7.3 is tabulated in Table 4.

A retuning of parameters affecting underlying event and minimum bias collisions is currently ongoing.

5 Other changes

Besides the major physics improvements highlighted in the previous sections, we have also made a number of smaller changes to the code and build system. Please refer to the online documentation for a fully detailed description or contact the authors.

Recently, the first steps have been taken towards creating HADML a machine learning hadronization model [35] and a protocol for fitting it to unbinned experimental data [36]. Although the model is still incomplete it has been successfully interfaced with Herwig. Once the model is finalized, it is planned to release it with Herwig.

6 Example results

Herwig 7.3 has been thoroughly validated against a wide range of existing data, as implemented in the Rivet and FastJet frameworks[37,38]. Parameter tuning has been performed using Professor [34].

A wide range of further plots can be found at https://herwig.hepforge.org/plots/herwig7.3.

Table 4 Tuned parameters in Herwig 7.3 vs Herwig 7.2, as outlined in [26]

Tuned parameter	Description	Herwig 7.3.0	Herwig 7.2.0
ClMaxLight [GeV]	Maximum allowable cluster mass for light quarks	3.529	3.649
ClPowLight	Power exponent for the mass of clusters with light quarks	1.849	2.780
PSplitLight	Parameter affecting the mass splitting for clusters with light quarks	0.914	0.899
PwtSquark	Probability for a $s\bar{s}$ quark pair to be spawned during cluster splittings	0.374	0.292
PwtDIquark	Probability for quarks forming a di-quark	0.331	0.298
SngWt	Weighting factor for singlet baryons in hadronization	0.891	0.740
DecWt	Weighting factor for decuplet baryons in hadronization	0.416	0.620
ProbabilityPowerFactor	Exponential factor in the ClusterFissioner probability function	6.486	–
ProbabilityShift	Offset in the ClusterFissioner probability function	− 0.879	–
KineticThresholdShift [GeV]	Adjustment to the kinetic threshold in ClusterFissioner	0.088	–
AlphaIn	Initial value for the strong coupling constant at $M_{Z^0} = 91.1876$ GeV	0.102	0.126
pTmin [GeV]	Minimum transverse momentum in parton shower	0.655	0.958

7 Summary and outlook

We have described a new release, version 7.3, of the Herwig event generator. This new release contains a number of improvements to both perturbative and non-perturbative simulation of collider physics and will form the basis of further improvements to both physics and technical aspects.

Acknowledgements We are indebted to Leif Lönnblad for his authorship of ThePEG, on which Herwig is built, and his close collaboration, and to the authors of Rivet, P8I and Professor. We are also grateful to Malin Sjödahl for providing the ColorFull library for distribution along with Herwig.

Funding This work was supported in part by the European Union as part of the H2020 Marie Skłodowska-Curie Initial Training Networks MCnetITN3 (Grant agreement no. 722104) and the UK Science and Technology Facilities Council (Grant numbers ST/T001011/1, ST/T001038/1). A.P. acknowledges support by the National Science Foundation under Grant no. PHY 2210161. G.B. thanks the UK Science and Technology Facilities Council for the award of a studentship. The work of A.S. and J.W. was funded by Grant no. 2019/34/E/ST2/00457 of the National Science Centre, Poland. A.S. was also supported by the Priority Research Area Digiworld under the program Excellence Initiative-Research University at the Jagiellonian University in Cracow. This work has been supported by the BMBF under Grant number 05H21VKCCA.

Data availability statement My manuscript has no associated data. [Author's' comment: Data sharing not applicable to this article as no datasets were generated or analysed during the current study.]

Code availability statement My manuscript has associated code/software in a data repository. [Author's comment: The software described in this paper, as well as earlier versions, is available from the website https://herwig.hepforge.org/.]

Funded by SCOAP[3].

References

1. J. Bellm et al., Herwig 7.0/Herwig++ 3.0 release note. Eur. Phys. J. **C76**, 196 (2016). https://doi.org/10.1140/epjc/s10052-016-4018-8. arXiv:1512.01178
2. J. Bellm et al., Herwig 7.1 Release Note. arXiv:1705.06919
3. J. Bellm et al., Herwig 7.2 release note. Eur. Phys. J. C **80**, 452 (2020). https://doi.org/10.1140/epjc/s10052-020-8011-x. arXiv:1912.06509
4. M. Bähr et al., Herwig++ physics and manual. Eur. Phys. J. Ser. C **58**, 639–707 (2008). https://doi.org/10.1140/epjc/s10052-008-0798-9. arXiv:0803.0883
5. M. Bähr et al., Herwig++ 2.2 release note. arXiv:0804.3053
6. M. Bähr et al., Herwig++ 2.3 release note. arXiv:0812.0529
7. S. Gieseke et al., Herwig++ 2.5 release note. arXiv:1102.1672
8. K. Arnold et al., Herwig++ 2.6 release note. arXiv:1205.4902
9. J. Bellm et al., Herwig++ 2.7 release note. arXiv:1310.6877
10. ATLAS Collaboration, G. Aad et al., Measurements of the Higgs boson production and decay rates and coupling strengths using pp collision data at $\sqrt{s} = 7$ and 8 TeV in the ATLAS experiment. Eur. Phys. J. C **76**, 6 (2016). https://doi.org/10.1140/epjc/s10052-015-3769-y. arXiv:1507.04548
11. ATLAS Collaboration, M. Aaboud et al., Search for Higgs bosons produced via vector-boson fusion and decaying into bottom quark pairs in $\sqrt{s} = 13$ TeV pp collisions with the ATLAS detector. Phys. Rev. D **98**, 052003 (2018). https://doi.org/10.1103/PhysRevD.98.052003. arXiv:1807.08639
12. M.R. Masouminia, P. Richardson, Implementation of angularly ordered electroweak parton shower in Herwig 7. JHEP **04**, 112 (2022). https://doi.org/10.1007/JHEP04(2022)112. arXiv:2108.10817

13. S. Gieseke, P. Stephens, B. Webber, New formalism for QCD parton showers. JHEP Ser. **12**, 045 (2003). https://doi.org/10.1088/1126-6708/2003/12/045. arXiv:hep-ph/0310083
14. D. Reichelt, P. Richardson, A. Siódmok, Improving the simulation of quark and gluon jets with Herwig 7. Eur. Phys. J. C Ser. **77**, 876 (2017). https://doi.org/10.1140/epjc/s10052-017-5374-8. arXiv:1708.01491
15. G. Bewick, S. Ferrario Ravasio, P. Richardson, M.H. Seymour, Logarithmic accuracy of angular-ordered parton showers. JHEP **04**, 019 (2020). https://doi.org/10.1007/JHEP04(2020)019. arXiv:1904.11866
16. G. Bewick, S. Ferrario Ravasio, P. Richardson, M.H. Seymour, Initial state radiation in the Herwig 7 angular-ordered parton shower. JHEP **01**, 026 (2022). https://doi.org/10.1007/JHEP01(2022)026. arXiv:2107.04051
17. S. Catani, S. Dittmaier, Z. Trócsányi, One-loop singular behaviour of QCD and SUSY QCD amplitudes with massive partons. Phys. Lett. Ser. B **500**, 149–160 (2001). arXiv:hep-ph/0011222
18. S. Dawson, The effective W approximation. Nucl. Phys. B Ser. **249**, 42–60 (1985). https://doi.org/10.1016/0550-3213(85)90038-0
19. N. Darvishi, M.R. Masouminia, Electroweak radiative corrections in precision LHC measurements of $W^{\pm}Z^{0}$+jets. Nucl. Phys. B Ser. **985**, 116025 (2022). https://doi.org/10.1016/j.nuclphysb.2022.116025. arXiv:2112.15487
20. N. Darvishi, M.R. Masouminia, Signature of the maximally symmetric 2HDM via $W^{\pm}/Z$-quadruplet productions at the LHC. Phys. Rev. D Ser. **103**, 095031 (2021). https://doi.org/10.1103/PhysRevD.103.095031. arXiv:2012.14746
21. ATLAS Collaboration, M. Aaboud et al., Measurement of W boson angular distributions in events with high transverse momentum jets at $\sqrt{s} = 8$ TeV using the ATLAS detector. Phys. Lett. B **765**, 132–153 (2017). https://doi.org/10.1016/j.physletb.2016.12.005. arXiv:1609.07045
22. J. Alwall, M. Herquet, F. Maltoni, O. Mattelaer, T. Stelzer, MadGraph 5: going beyond. JHEP Ser. **1106**, 128 (2011). https://doi.org/10.1007/JHEP06(2011)128. arXiv:1106.0522
23. S. Catani, B.R. Webber, G. Marchesini, QCD coherent branching and semiinclusive processes at large x. Nucl. Phys. Ser. B **349**, 635–654 (1991). https://doi.org/10.1016/0550-3213(91)90390-J
24. ATLAS Collaboration, G. Aad et al., Measurement of the transverse momentum and ϕ^{*}_{η} distributions of Drell–Yan lepton pairs in proton–proton collisions at $\sqrt{s} = 8$ TeV with the ATLAS detector. Eur. Phys. J. C **76**, 291 (2016). https://doi.org/10.1140/epjc/s10052-016-4070-4. arXiv:1512.02192
25. A.F. Falk, M.E. Peskin, Production, decay, and polarization of excited heavy hadrons. Phys. Rev. D Ser. **49**, 3320–3332 (1994). https://doi.org/10.1103/PhysRevD.49.3320. arXiv:hep-ph/9308241
26. M.R. Masouminia, P. Richardson, Hadronization and decay of excited heavy hadrons in Herwig 7. JHEP **07**, 278 (2024). https://doi.org/10.1007/JHEP07(2024)278. arXiv:2312.02757
27. A.F. Falk, M.E. Luke, Strong decays of excited heavy mesons in chiral perturbation theory. Phys. Lett. B Ser. **292**, 119–127 (1992). https://doi.org/10.1016/0370-2693(92)90618-E. arXiv:hep-ph/9206241
28. A.F. Falk, T. Mehen, Excited heavy mesons beyond leading order in the heavy quark expansion. Phys. Rev. D Ser. **53**, 231–240 (1996). https://doi.org/10.1103/PhysRevD.53.231. arXiv:hep-ph/9507311
29. Belle Collaboration, V. Balagura et al., Observation of $D_{s1}(2536)^{+} \to D^{+}\pi^{-}K^{+}$ and angular decomposition of $D_{s1}(2536)^{+} \to D^{*+}K^{0}_{S}$. Phys. Rev. D**77**, 032001 (2008). https://doi.org/10.1103/PhysRevD.77.032001. arXiv:0709.4184
30. A.H. Hoang, O.L. Jin, S. Plätzer, D. Samitz, Matching hadronization and perturbative evolution: the cluster model in light of infrared shower cutoff dependence. arXiv:2404.09856
31. Particle Data Group Collaboration, R.L. Workman et al., Review of particle physics. PTEP **2022**, 083C01 (2022). https://doi.org/10.1093/ptep/ptac097
32. Particle Data Group Collaboration, W.M. Yao et al., Review of particle physics. J. Phys. G **33**, 1–1232 (2006). https://doi.org/10.1088/0954-3899/33/1/001
33. L. Lönnblad et al. TheP8I: an interface between the Pythia8 and the ThePEG toolkit. https://gitlab.cern.ch/TheP8I
34. A. Buckley, H. Hoeth, H. Lacker, H. Schulz, J.E. von Seggern, Systematic event generator tuning for the LHC. Eur. Phys. J. Ser. C **65**, 331–357 (2010). https://doi.org/10.1140/epjc/s10052-009-1196-7. arXiv:0907.2973
35. A. Ghosh, X. Ju, B. Nachman, A. Siódmok, Towards a deep learning model for hadronization. Phys. Rev. D Ser. **106**, 096020 (2022). https://doi.org/10.1103/PhysRevD.106.096020. arXiv:2203.12660
36. J. Chan, X. Ju, A. Kania, B. Nachman, V. Sangli, A. Siódmok, Fitting a deep generative hadronization model. JHEP Ser. **09**, 084 (2023). https://doi.org/10.1007/JHEP09(2023)084. arXiv:2305.17169
37. A. Buckley et al., Rivet user manual. Comput. Phys. Commun. Ser. **184**, 2803–2819 (2013). https://doi.org/10.1016/j.cpc.2013.05.021. arXiv:1003.0694
38. M. Cacciari, G.P. Salam, G. Soyez, FastJet user manual. Eur. Phys. J. Ser. **C72**, 1896 (2012). https://doi.org/10.1140/epjc/s10052-012-1896-2. arXiv:1111.6097